AGU PUBLICATIONS

JGR

Journal of Geophysical Research: Space Physics

RESEARCH ARTICLE

10.1002/2014JA020136

Key Points:
- Ordering the ionospheric convection by static IMF parameters is inadequate
- IMF history is important in governing coupled magnetosphere-ionosphere dynamics
- Long, steady intervals of IMF continue to modify the ionospheric convection

Supporting Information:
- Readme
- Figure S1
- Figure S2

Correspondence to:
A. Grocott,
a.grocott@lancaster.ac.uk

Citation:
Grocott, A., and S. E. Milan (2014), The influence of IMF clock angle timescales on the morphology of ionospheric convection, *J. Geophys. Res. Space Physics*, *119*, doi:10.1002/2014JA020136.

Received 28 APR 2014
Accepted 2 JUL 2014
Accepted article online 5 JUL 2014

The influence of IMF clock angle timescales on the morphology of ionospheric convection

A. Grocott[1] and S. E. Milan[2]

[1]Department of Physics, Lancaster University, Lancaster, UK, [2]Department of Physics and Astronomy, University of Leicester, Leicester, UK

Abstract We exploit a database of high-latitude ionospheric electric potential patterns, derived from radar observations of plasma convection in the Northern Hemisphere from the years 2000–2006, to investigate the timescales of interplanetary magnetic field (IMF) control of ionospheric convection and associated magnetospheric dynamics. We parameterize the convection observations by IMF clock angle, θ (the angle between geocentric solar magnetic (GSM) north and the projection of the IMF vector onto the GSM *Y-Z* plane), and by an IMF timescale, τ_B (the length of time that a similar clock angle has been maintained prior to the convection observations being made). We find that the nature of the ionospheric convection changes with IMF clock angle, as expected from previous time-averaged studies, and that for τ_B ~30 min, the convection patterns closely resemble their time-averaged counterparts. However, as τ_B increases we find that the convection evolves away from the time-averaged patterns to reveal modified characteristic flow features. We discuss these findings in terms of solar wind-magnetosphere-ionosphere coupling and consider their implications for understanding the time-dependent nature of magnetospheric dynamics.

1. Introduction

Magnetic reconnection between the interplanetary and terrestrial magnetic fields drives convection of plasma and magnetic flux in the coupled magnetosphere-ionosphere system [*Dungey*, 1961]. The nature of this convection is known to be governed by both the strength and orientation of the interplanetary magnetic field (IMF) [e.g., *Heppner and Maynard*, 1987; *Rich and Hairston*, 1994; *Weimer*, 1995; *Ruohoniemi and Greenwald*, 1996, 2005] with the timescale for the dayside ionosphere to respond to IMF changes being of the order of just a few minutes [e.g., *Nishida*, 1968]. Some disagreement exists, however, as to how fast any changes propagate from the dayside ionosphere to other local times with some authors having suggested a global response on timescales of just seconds [*Ridley et al.*, 1998] and others having found delay times ranging from 10 to 15 min [e.g., *Lockwood et al.*, 1986; *Etemadi et al.*, 1988; *Todd et al.*, 1988; *Saunders et al.*, 1992; *Khan and Cowley*, 1999]. *Cowley and Lockwood* [1992] suggested a theoretical picture in which flow changes occurring in response to a change in the IMF propagate away from the dayside cusp region to establish a new steady state convection pattern over 10–15 min. Based solely on this, one might assume that for intervals of IMF that remain steady over such timescales, a simple evolution from one steady state to another would occur. Such an assumption has often been made in studies of the IMF dependence of the convection whereby 10–40 min intervals of the IMF parameters have been inspected to ensure a quasi-steady state has been approached [e.g., *Heppner and Maynard*, 1987; *Weimer*, 1995; *Ruohoniemi and Greenwald*, 1996; *Shepherd et al.*, 2002; *Ruohoniemi and Greenwald*, 2005].

A problem exists with this assumption, however, that is related to the storage-and-release component of the convection driver. In the widely accepted picture of *Dungey* [1961], reconnection also occurs in the magnetotail, closing the previously opened flux and returning it to the dayside to complete the cycle of convection commonly referred to as the Dungey cycle. Although some studies have suggested that a steady state can be approached via this mechanism [e.g., *Sergeev et al.*, 1996], it is often the case that the magnetotail stores the open flux that is added at the dayside, for some variable amount of time, before releasing it during episodic tail reconnection associated with processes such as substorms [e.g., *Hones*, 1979; *Baker et al.*, 1996]. As discussed by *Lockwood et al.* [1990] and *Cowley and Lockwood* [1992], these tail processes give rise to a time dependency of the convection that is more complex owing to the variable timescales over which they occur. *Lester et al.* [1993] and *Hairston and Heelis* [1995], for example, both reported longer timescales of

~30–60 min for the development of the flow pattern as a whole. In the case of geomagnetic storms, it may take even longer for the flows to evolve [e.g., *Hutchinson et al.*, 2011b]. This complexity of the nightside contribution to the convection has been studied in detail by *Grocott et al.* [2009, 2010] who have developed the existing IMF characterization of the convection patterns to incorporate the effects of these time-dependent tail processes.

While the above considerations do then take into account the time dependency of the system over timescales of a few hours that are typical of the substorm cycle, they do not account for changes over the full ~12 h cycle time of the Dungey cycle [*Cowley et al.*, 2003]. Substorms, for example, are known to only close of the order of a third of the open flux present in the magnetosphere in any one cycle [*Milan et al.*, 2007], with the exact amount closed varying in accordance with the strength of the dayside driving [*Milan et al.*, 2008]. Other phenomena, such as tail reconnection during IMF northward, nonsubstorm intervals (TRINNIs) [*Grocott et al.*, 2007], are understood to close even less flux, of the order ~20% [e.g., *Milan et al.*, 2006]. The history of the IMF may therefore be expected to play a role in governing the dynamics of the system for timescales of anywhere up to 12 h, given that its influence may persist on open and newly closed flux during this time. This is particularly likely in respect to the influence of IMF B_Y (i.e., the dusk-dawn component defined in, for example, geocentric solar magnetospheric coordinates, or GSM), which is known to introduce a dusk-dawn asymmetry into the coupled magnetosphere-ionosphere system and which tends to demonstrate a longer characteristic timescale in the system than B_Z. This has been demonstrated by *Grocott et al.* [2010] and *Milan et al.* [2010] who found that the location of substorm onset and the morphology of the associated nightside flows are influenced by the time history of IMF B_Y over timescales of tens of hours. It is also consistent with the results of *Murr and Hughes* [2007] who investigated the coherence between variations in the IMF and those in the ionospheric equivalent flow (determined from magnetometer data) over short (~20 min) timescales. They found that the coherence was lower for IMF B_Y than for B_Z, suggesting a less direct relationship in the case of the former.

While it may be true, therefore, that ~20 min is adequate to produce a reconfiguration of the coupled magnetosphere-ionosphere system following a change in the IMF, it would seem that a persistence of IMF B_Y will result in a continued evolution of the system over longer timescales. This was suggested by the study of *Grocott et al.* [2008] who found that the nightside portion of the convection pattern, in particular, could develop much stronger asymmetries than previous studies indicated, if subject to intervals where one sense of B_Y had dominated the IMF for at least 2 h. However, *Grocott et al.* [2008] identified the asymmetric flows first, and then analyzed the concurrent IMF conditions with which they were associated. As pointed out by *Murr and Hughes* [2007], to properly study the dynamics of the convection pattern in response to a time variation in the IMF, one ideally requires a time sequence of the ionospheric flow pattern, the latter being difficult to quantify. *Grocott et al.* [2012] discussed a method by which this can be achieved, using the coefficients of a spherical harmonic expansion of the ionospheric electric potential, which provides a quantitative deconstruction of the ionospheric flows. In this paper, we utilize this method to investigate the effects of solar wind-magnetosphere-ionosphere coupling over various timescales.

2. Observations

Our observations are based on an archive of sixth-order spherical harmonic coefficients, spanning the years 2000–2006, that describe the large-scale ionospheric electric potential pattern in the Northern Hemisphere, which is equivalent to the pattern of $\mathbf{E} \times \mathbf{B}$ plasma convection. These coefficients are derived from measurements of the ionospheric flow made by the Super Dual Auroral Radar Network (SuperDARN) [*Ruohoniemi and Baker*, 1998; *Chisham et al.*, 2007] and are described in detail by *Grocott et al.* [2012]. The use of the coefficients enables the large-scale nature of the convection to be studied (in comparison to small-scale structures than might be better resolved in the raw radar velocity measurements) and enables simple comparison with previous results that utilize the same analysis technique. We compare the convection observations (provided at 2 min time resolution) to 2 min averages of IMF data provided by the Magnetic Field Experiment [*Smith et al.*, 1998] on the Advanced Composition Explorer (ACE) spacecraft [*Stone et al.*, 1998]. These IMF data have been time lagged to the dayside ionosphere using the method of *Khan and Cowley* [1999].

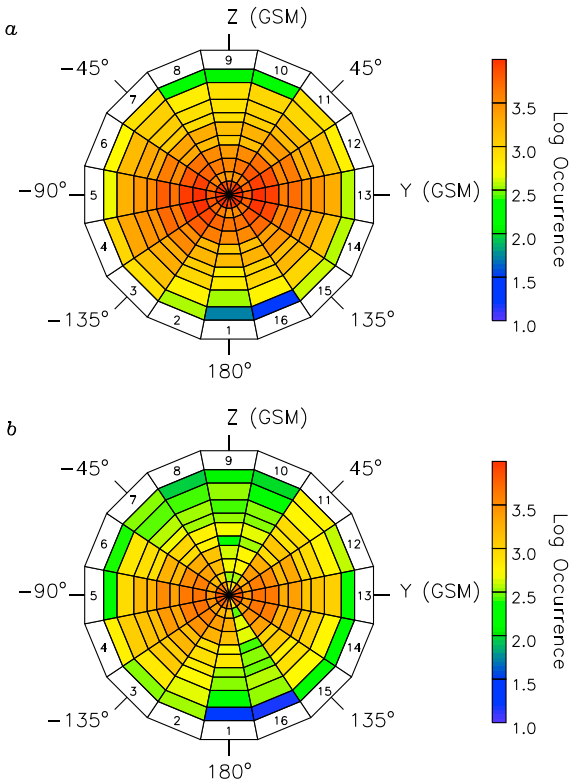

Figure 1. Occurrence distributions of convection data, sorted according to IMF clock angle (θ) sector and IMF timescale (τ_B) bin. The IMF sector number, *i*, corresponding to an IMF range $\theta = [22.5(i-8)\pm22.5]°$, is indicated around the edge of the plot. With radius from the center of the plot, τ_B increases and has boundaries at 20 min (at the center), 30, 40, 60, 90, 120, 180, 240, 360, and 600 min. The outermost bin corresponds to $\tau_B > 600$ min. Shown color coded on a log scale according to the color bars on the right are (a) the occurrence for all IMF magnitudes and (b) the occurrence after filtering by IMF magnitude (as described in the text).

2.1. IMF Sorting of the Convection Data

The IMF data have been used to bin our convection data into 16 IMF clock angle sectors, illustrated by the numbered sectors in both panels of Figure 1. The clock angle, θ, is defined as the angle between geomagnetic north and the projection of the IMF vector onto the GSM *Y-Z* plane ($\theta = \arctan(B_Y, B_Z)$) and is defined for $-180° < \theta \leq 180°$. For ease of presentation, the bins are represented by 22.5° sectors in the figure; however, they are actually 45° wide in order to provide sufficient statistics. The eight odd-numbered IMF sectors match those used by *Ruohoniemi and Greenwald* [2005] and enable direct comparison with their results. The eight even-numbered sectors, which overlap the odd sectors by 22.5°, enable an alternative inspection of the IMF dependence of the convection as discussed below.

In addition to the traditional clock angle binning, our convection data have also been binned according to an IMF timescale, τ_B, presented radially in Figure 1. In minutes, τ_B is defined as the time that the IMF has been consistently within a given clock angle sector. To prevent brief excursions out of a given sector from impacting the statistics for larger τ_B, a threshold of 90% has been applied to the "consistency" definition. For example, if during a 60 min interval the IMF remained in a single sector for a total of no less than 54 min, then we consider consistency to have been maintained. Ten bins of τ_B are defined, with boundaries at 20 min (the center of each plot in Figure 1), 30, 40, 60, 90, 120, 180, 240, 360, and 600 min, with the final, outermost bin being $\tau_B > 600$ min. For each 2 min interval, we tag the convection data with the coincident IMF sector and its corresponding timescale bin. We limit the shortest timescale bin to 20 min because as discussed in section 1, this is the timescale below which we would not expect the convection pattern to have fully adjusted to any instantaneous change in the IMF. We are interested in longer timescale effects on the convection, not variability associated with the propagation of instantaneous IMF changes around the polar cap.

After determining the appropriate $\theta - \tau_B$ bin for each 2 min interval, we further reduce our data to account for limitations in radar data coverage and variations in IMF magnitude. We first exclude intervals for which there were fewer than 250 radar measurements to constrain the convection patterns. Setting such a limit minimizes the effects of limited radar data coverage on the derived convection patterns while maintaining adequate statistics in the least populous $\theta - \tau_B$ bins. This process is similar to that used in previous studies [e.g., *Shepherd et al.*, 2002; *Grocott et al.*, 2012], and we discuss its implications further below. The occurrence distribution of convection data thus remaining is represented by the color coding in Figure 1a, which shows the occurrence of 2 min intervals in each clock angle and τ_B bin. These data reveal that the most common clock angle sectors are those around ±90°, consistent with the average orientation of the Parker spiral field [*Parker*, 1963]. They also reveal the decrease in occurrence with increasing IMF timescale. This is to be expected, and in fact, we choose unequal τ_B bin widths in anticipation of this; our bins get wider with

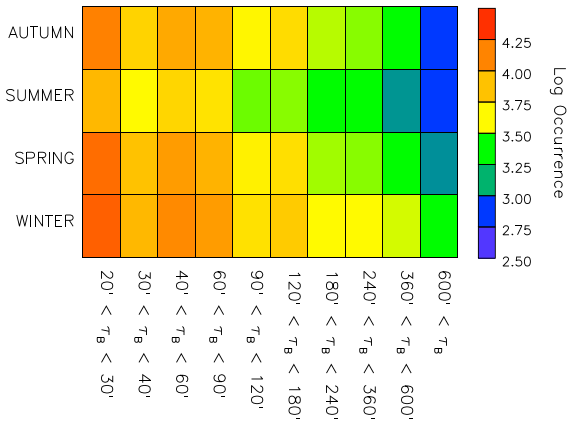

Figure 2. Occurrence distributions of convection data, sorted according to season and IMF timescale (τ_B) bin, and shown color coded on a log scale according to the color bar on the right.

increasing τ_B to make some effort to account for the decreasing occurrence. In this way we have reasonable statistics even at the least common end of the IMF timescale range.

The other factor we account for is the variable IMF magnitude (in the GSM *Y-Z* plane), B_{YZ}. In previous studies, such as *Ruohoniemi and Greenwald* [2005], they subdivided their statistics by IMF magnitude in addition to clock angle. Owing to the fact that we already subdivide our statistics by IMF timescale, it is difficult to further subdivide by magnitude without compromising our statistics at the longest timescales. However, the effects of IMF magnitude on the convection patterns are significant [e.g., *Ruohoniemi and Greenwald*, 2005] and must be accounted for in our study. We therefore subdivide by the same magnitude ranges employed by *Ruohoniemi and Greenwald* [2005], i.e., 0–3 nT, 3–5 nT, and 5–10 nT (with the addition of an extra bin spanning 10–20 nT to better differentiate the convection patterns in the high-B_{YZ} regime) but only consider that range containing the most data in the least populous timescale bin (in each clock angle sector). In other words, for each clock angle sector, we simply determine which IMF magnitude bin we must use to maximize the statistics at long timescales. The resulting occurrence distributions, shown in Figure 1b, indicate that most of our 160 $\theta - \tau_B$ bins contain at least ~500 intervals, with only seven bins containing fewer than ~200. These low-occurrence bins are therefore treated with caution and are excluded from our subsequent discussion and interpretation.

Lastly, we also investigated the seasonal distribution of our data to determine the likelihood that dipole tilt variations, known to influence the nature of the convection [e.g., *Pettigrew et al.*, 2010], might affect our results. The results of this analysis are presented in Figure 2 which shows the occurrence distribution of our data plotted as a function of τ_B and season, color coded in a similar fashion to the data in Figure 1. These results show that there is a seasonal trend in the data distribution, having a peak occurrence in winter and a trough in summer of about one third that of the winter peak. This trend is fairly consistent over the different timescale bins and is also consistent with the expected seasonal variation in SuperDARN scatter [*Ruohoniemi and Greenwald*, 1997]. It is thus likely to be predominantly an instrumental effect rather than being due to any relationship between season and timescale. We can therefore conclude that while there may be a general seasonal effect in our results, this effect should be similar at all timescales and thus not contaminating any trends we observe. At the longer timescale end of the distribution, there may be a slight trend for the winter bias to become more pronounced; hence, if any seasonal dependence is present in our results, we would expect this to be consistent with Northern Hemisphere winter effects. The implications of this are discussed in section 3.

2.2. Average Convection Patterns

For each of the 160 $\theta - \tau_B$ bins indicated in Figure 1, we have computed an average convection pattern by taking the mean of each spherical harmonic coefficient of the fit and reconstructing the resulting potential pattern. To scale the patterns appropriately, in terms of their latitudinal extent, we have also taken the mean of the equatorward boundary latitudes from each convection pattern. A detailed description of the derivation of this latitude is given by *Shepherd and Ruohoniemi* [2000]. An example set of the resulting patterns, which correspond to the eight odd-numbered IMF sectors (see Figure 1) and the smallest IMF timescale range (20–30 min), is illustrated in Figure 3. These are presented in a similar format to Figure 7 of *Ruohoniemi and Greenwald* [2005], for easy comparison. In each panel, the potential contours are plotted in a magnetic local time-magnetic latitude coordinate system with noon to the top and dusk to the left. Negative electric potentials are colored blue and positive potentials orange, as indicated by the color bar on the right. The minimum and maximum potentials are also indicated in the bottom left- and right-hand sides of each panel, respectively, and the low-latitude extent of the convection is indicated with a simple circle labeled toward

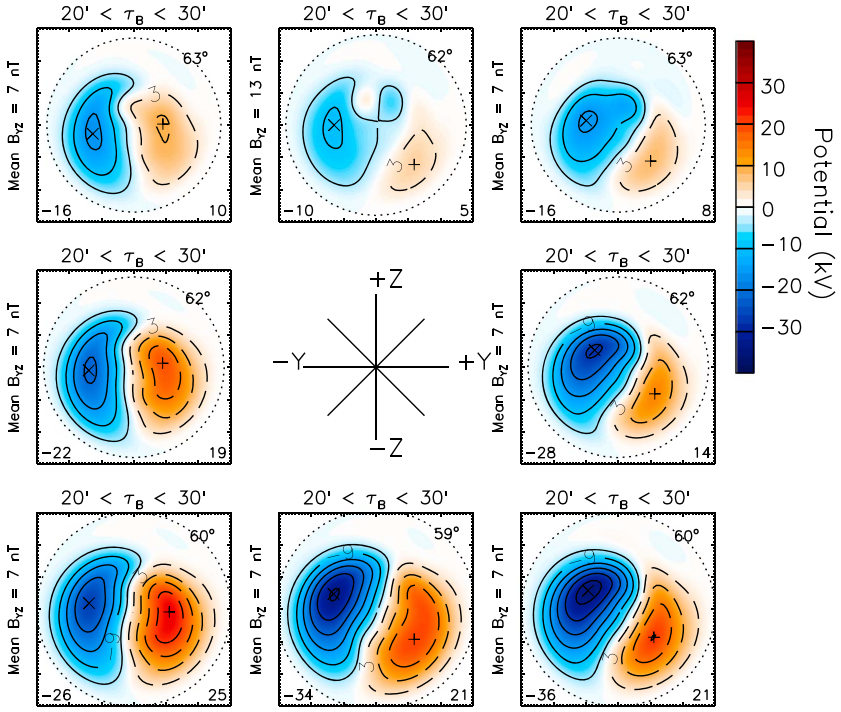

Figure 3. Maps of the ionospheric convection for the τ_B range 20 min < τ_B < 30 min, for the eight odd-numbered IMF θ sectors shown in Figure 1. In each panel, the potential contours, color coded according to the bar on the right, are plotted in a magnetic local time-magnetic latitude coordinate system with noon to the top and dusk to the left. The minimum and maximum potentials are indicated in the bottom left- and right-hand sides of each panel, respectively. The low-latitude extent of the convection is indicated by the dotted circle labeled toward the top right of each plot. The τ_B bin is indicated on the top of each panel and the mean IMF magnitude, B_{YZ} is indicated on the left.

the top right of each plot. In this, and subsequent figures, the τ_B bin is indicated on the top of each panel (in this case 20–30 min for every panel) and the mean value of B_{YZ} is indicated on the left.

The patterns shown in this figure are very similar to those in Figure 7 of *Ruohoniemi and Greenwald* [2005], as might be expected given the similar criteria used in their derivation. Where differences are apparent they may be attributed to a number of factors, the most significant of which are addressed below. One concerns the IMF magnitude: as described above, *Ruohoniemi and Greenwald* [2005] inspected all B_{YZ} bins, whereas our subdivision by τ_B means we have had to focus on a single magnitude bin in each case. Our Figure 3 therefore contains data from a variety of B_{YZ} ranges (although in fact only the $+Z$ clock angle bin has a significantly different B_{YZ} in this case; this is discussed further in section 2.2.3). A second factor is the most relevant to the present study: *Ruohoniemi and Greenwald* [2005] used intervals where the same IMF conditions must have prevailed for at least, but possibly much longer than, 36 min. Their patterns will therefore also include the averaged effects of much longer intervals of steady IMF, which are exactly the effects we are interested in elucidating and are what we focus on in the remainder of this paper. We choose four IMF clock angle regimes to study in detail: strongly southward IMF (B_Z-), strongly northward IMF (B_Z+), and two intermediate clock angle regimes, where B_Z is northward, but B_Y is dominant (both for duskward and dawnward IMF orientations). The reasons for our particular choice of these latter two regimes is based in part on an initial inspection of all the data (to identify if particular clock angle regimes exhibited a significant timescale effect) and in part on the results of earlier work, discussed below.

2.2.1. Southward IMF

We begin our analysis of the effect of IMF timescale by considering the case for strictly southward IMF: $-157.5° > \theta > 157.5°$, or IMF sector 1 (as defined in Figure 1). An average convection map for each of the τ_B bins is presented in Figure 4, with each panel presented in the same format as those in Figure 3. Very little difference in the shape of the convection pattern is evident for the different timescales; however, the latitudinal extent of the patterns does increase with increasing timescale. It would seem then that although there is no integrated effect of a southward IMF on the convection pattern shape, a persistent southward IMF of

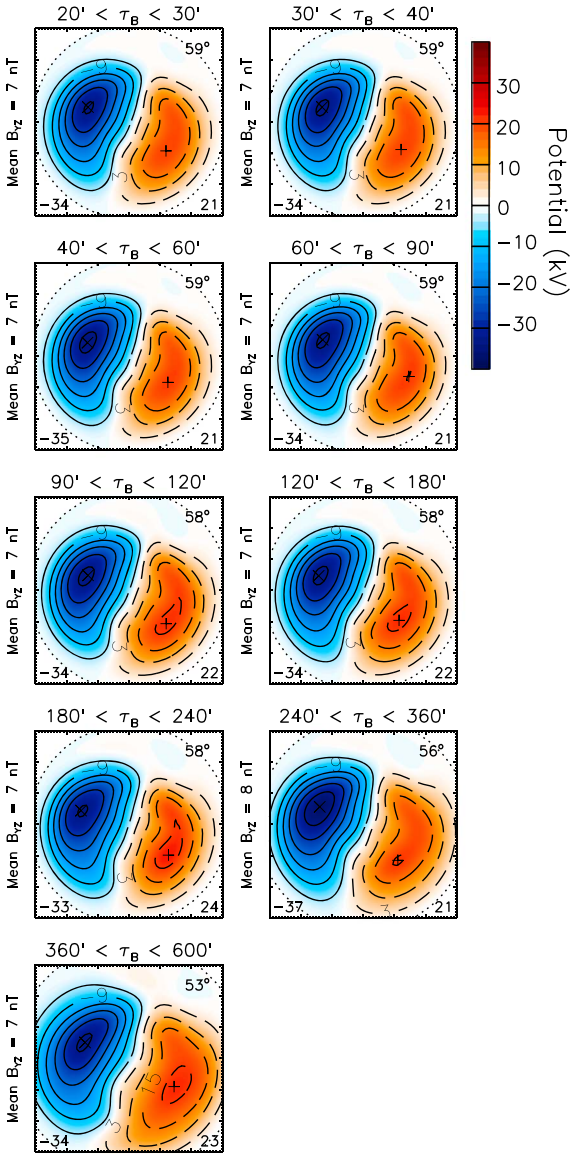

Figure 4. Maps of the ionospheric convection, in a similar format to Figure 3, for the clock angle range $-157.5° > \theta > 157.5°$ (sector 1), for the nine bins of τ_B satisfying the threshold criterion described in the text.

magnitude of 5–10 nT results in the size of the pattern increasing at an average rate of ~0.5°/h. Lastly, there is a small increase in the overall strength of the convection (evidenced by an increase in electric potentials); this is discussed further below.

If we consider the other IMF sectors that have a southward B_Z component, with the addition of a nonzero B_Y component (sectors 2–4 and 14–16, in the supporting information), we find even less evolution of the patterns with increasing IMF timescale. There is some indication of a small rotation of the patterns between the shortest and longest timescales, for certain IMF sectors, but the significance is not clear from an inspection of these patterns alone. This suggests that for southward IMF orientations, the magnetosphere is quickly able to reach an equilibrium state such that there is little effect of prolonged intervals of driving by the solar wind under these circumstances. All of these average patterns are included as supporting information for reference.

2.2.2. Northward IMF With a Dominant B_Y Component

In Figure 5, we show the average convection patterns corresponding to (a) IMF sector 6 ($-90° < \theta < -45°$) and (b) IMF sector 12 ($45° < \theta < 90°$). In both cases, a clear evolution of the shape of the convection pattern is evident. In Figure 5a, the negative potential (dusk) cell becomes extended across the midnight sector and the positive potential (dawn) cell shrinks dramatically in size. In Figure 5b, it is the positive potential (dawn) cell that becomes more extended across the midnight sector (albeit less so than the dusk cell does in Figure 5a), and in this case, both potential cells shrink slightly. In both cases, the patterns also rotate with increasing τ_B. In Figure 5a, the orientation of the flows over the polar cap rotates to later local times from largely noon-midnight in the first τ_B bin to strongly postnoon to postmidnight in τ_B bin 10. In Figure 5b, the orientation remains prenoon to premidnight but rotates to earlier local times with increasing τ_B. In both cases, the overall size of the convection pattern shrinks by 3° with increasing τ_B (except for the tenth τ_B bin in Figure 5a, where it appears to have expanded again). Similar trends exist for IMF sectors 7 and 11 (see supporting information).

2.2.3. Strictly Northward IMF

In Figure 6, we show the average convection patterns corresponding to strongly northward IMF (sector 9: $-22.5° < \theta < 22.5°$). Yet again, there are clear differences between the patterns for short IMF timescales and those for longer timescales. Over the first eight τ_B bins, the pattern evolves from a distorted two-or-three-cell pattern, similar to that shown in Figure 7 of *Ruohoniemi and Greenwald* [2005], to a well-defined four-cell pattern typically expected for strongly northward IMF. This implies that it may take up to 6 h for the magnetosphere to fully adjust to such an orientation in terms of establishing a sustainable reverse convection pattern at high latitudes (although it should be noted that over timescales longer than

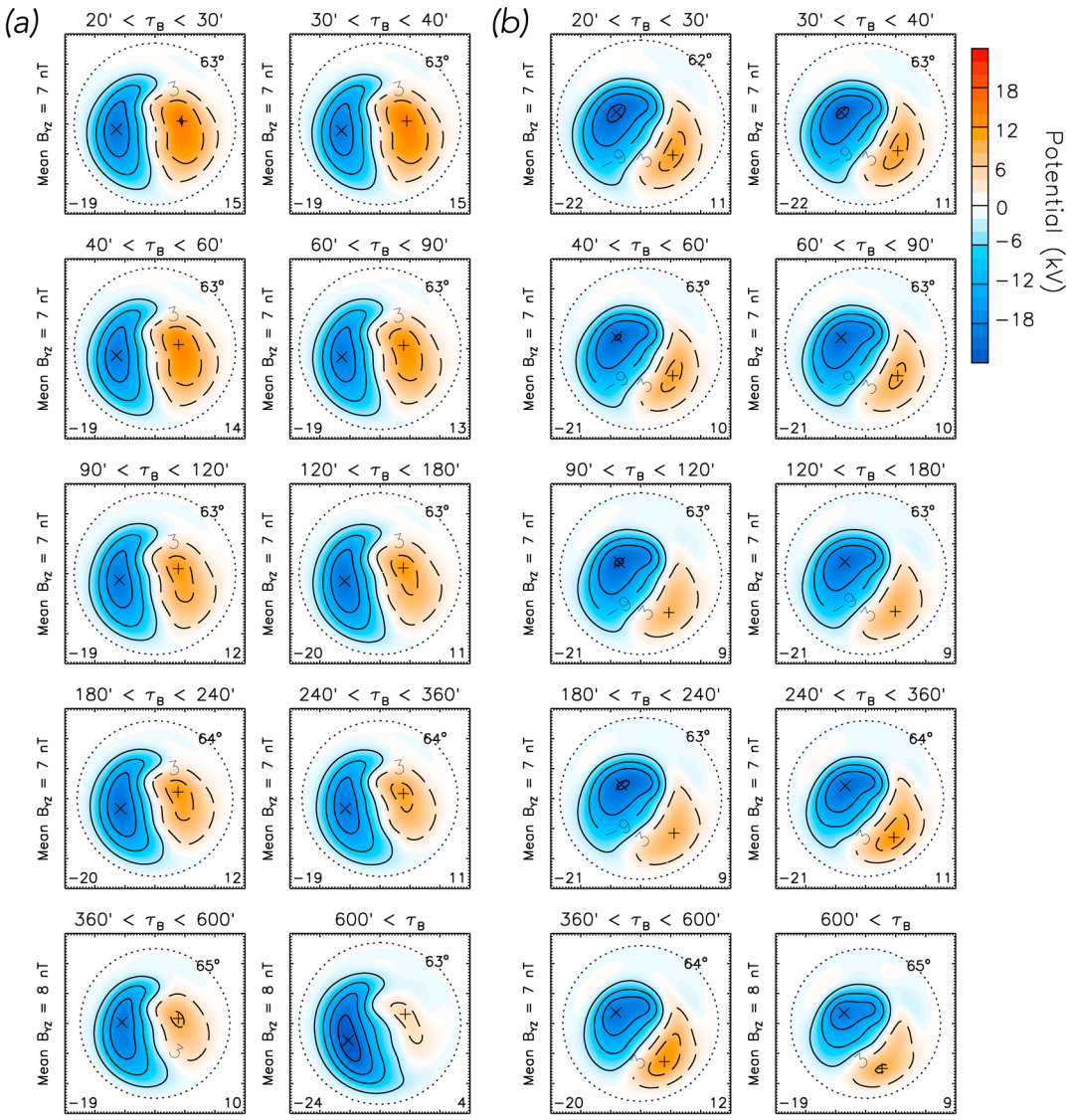

Figure 5. Maps of the ionospheric convection for the clock angle range (a) $-90° < \theta < 45°$ (sector 6) and (b) $45° < \theta < 90°$ (sector 12), in the same format as Figure 4.

this the strong reverse cells are not maintained). It is also worth commenting on the fact that the IMF magnitude is much larger for this clock angle bin. This is a result of the way in which IMF magnitude variability was controlled for (see section 2.1) and simply implies that the longest, steadily northward IMF intervals (that are inherently less common in our data set) happened to occur with large IMF magnitude. This might be due to the fact that such intervals were associated with a particular type of IMF structure, such as interplanetary coronal mass ejections. The details of this are not pertinent to the present study, only that the mean IMF magnitude for our subset of observations is quasi-constant at 13–14 nT. As such, changes in the convection patterns with τ_B should not be related to IMF magnitude variations.

2.3. Quantitative Deconstruction of the Patterns

The average patterns presented above provide a straightforward, but largely qualitative, means of inspecting the morphology of the convection for the different IMF sectors and steadiness timescales. The spherical harmonic coefficients that define these patterns, on the other hand, provide a simple way by which the full two-dimensional nature of the convection can be investigated quantitatively [e.g., *Grocott et al.*, 2012]. In this section, we use this technique to investigate the extent to which the different IMF timescales control the evolution of the convection pattern by inspecting the relationship between τ_B and some of the different spherical harmonic basis functions that describe the ionospheric electric potential (as illustrated, for

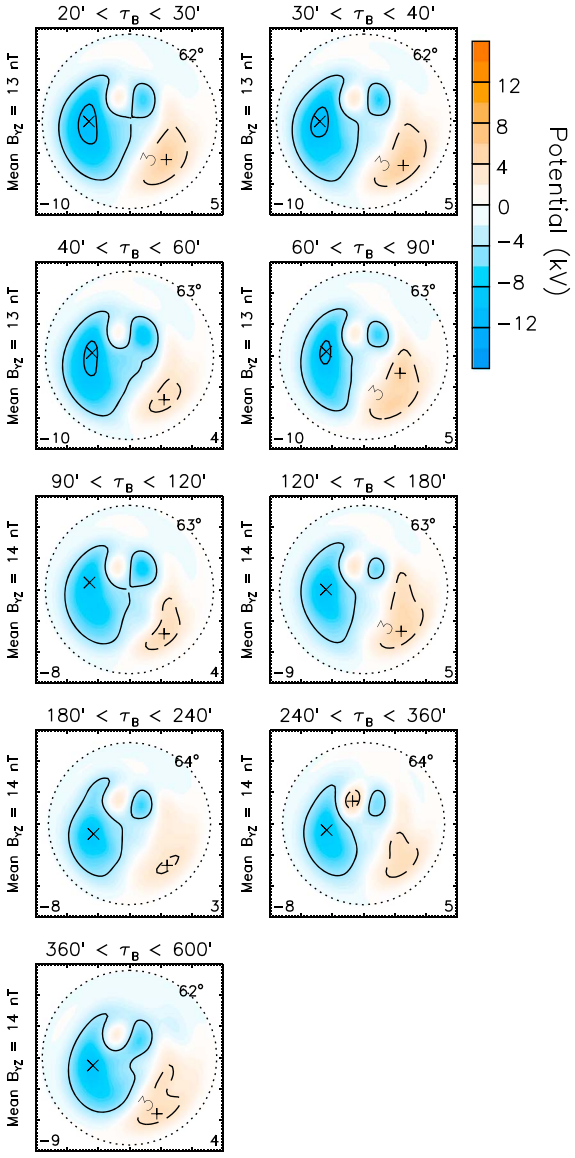

Figure 6. Maps of the ionospheric convection for the clock angle range $-22.5° < \theta < 22.5°$ (sector 9), in the same format as Figure 4.

example, in Figure 2 of *Grocott et al.* [2012]). Figure 7 provides a summary of our results for the four IMF sectors discussed in detail above. Figures 7a–7f present a selection of the spherical harmonic coefficients, $A_{l,m}$, up to order $l = 2$. In each panel, mean values of $A_{l,m}$ are plotted as a function of τ_B, with the order, l, and degree, m, of the corresponding basis function given at the top. The zeroth-degree ($m = 0$) basis functions have rotational symmetry, and so the corresponding values of $A_{l,m}$ are real valued. The higher-degree basis functions are parameterized by complex coefficients, which are represented here in terms of their magnitude, $|A_{l,m}|$, and phase, $\phi_{l,m}$. The magnitude corresponds to the strength of the corresponding basis function, in kV, and the phase corresponds to the rotation of the basis function about the pole, given in hours of magnetic local time.

For comparison with the coefficient data, we also show the more typically quoted parameters of the convection pattern. In Figure 7g, we show mean values of the maximum potential difference, $\Phi_{diff} = \Phi_{max} - \Phi_{min}$. This is often used as proxy for the strength of the convection. Its behavior certainly resembles that of the $|A_{1,1}|$ coefficient, which corresponds to the basic twin vortex basis function. In principle, however, different components of the flow may contribute to Φ_{diff} such that its precise physical significance cannot be rigidly defined. In Figure 7h, we show the residual potential, $\Phi_{res} = \Phi_{max} + \Phi_{min}$, which provides a measure of the asymmetry in the potential, typically between the dawn and dusk twin vortex convection cells. Lastly, Figure 7i shows mean values of the latitude of the equatorward boundary of the convection, Λ_0. In all the panels of Figure 7, the data are color coded as follows: sector 1 (B_Z-): orange, sector 6 (B_Y-): blue, sector 9 (B_Z+): red, and sector 12 (B_Y+): green. In each case, the solid lines provide an estimate of the upper and lower 95% confidence intervals for the means (with the dotted portions indicating where we discarded data that failed to meet our occurrence threshold). It is clear that in many cases, the trends apparent in the data are significant at the 95% confidence level.

Two obvious conclusions can be drawn from these results. The first is that the convection is dependent on IMF sector, exhibiting different morphologies for the four different sets of points. Consider, for example, the data in Figure 7c. These show that the magnitude of the $A_{1,1}$ coefficient is low for IMF-B_Z+, takes intermediate values for B_Y-dominated IMF, and is highest for B_Z-. This is largely consistent with the behavior of Φ_{diff} and with what we know about how the strength of the twin vortex convection pattern responds to the IMF clock angle; further details of this IMF dependence of the coefficients are discussed by *Grocott et al.* [2012] and are not considered further here. The second conclusion that can be drawn is that the convection is also strongly dependent on τ_B. This is consistent with the qualitative observations discussed above, which showed that the nature of the convection pattern changes over different IMF timescales. Using the results in

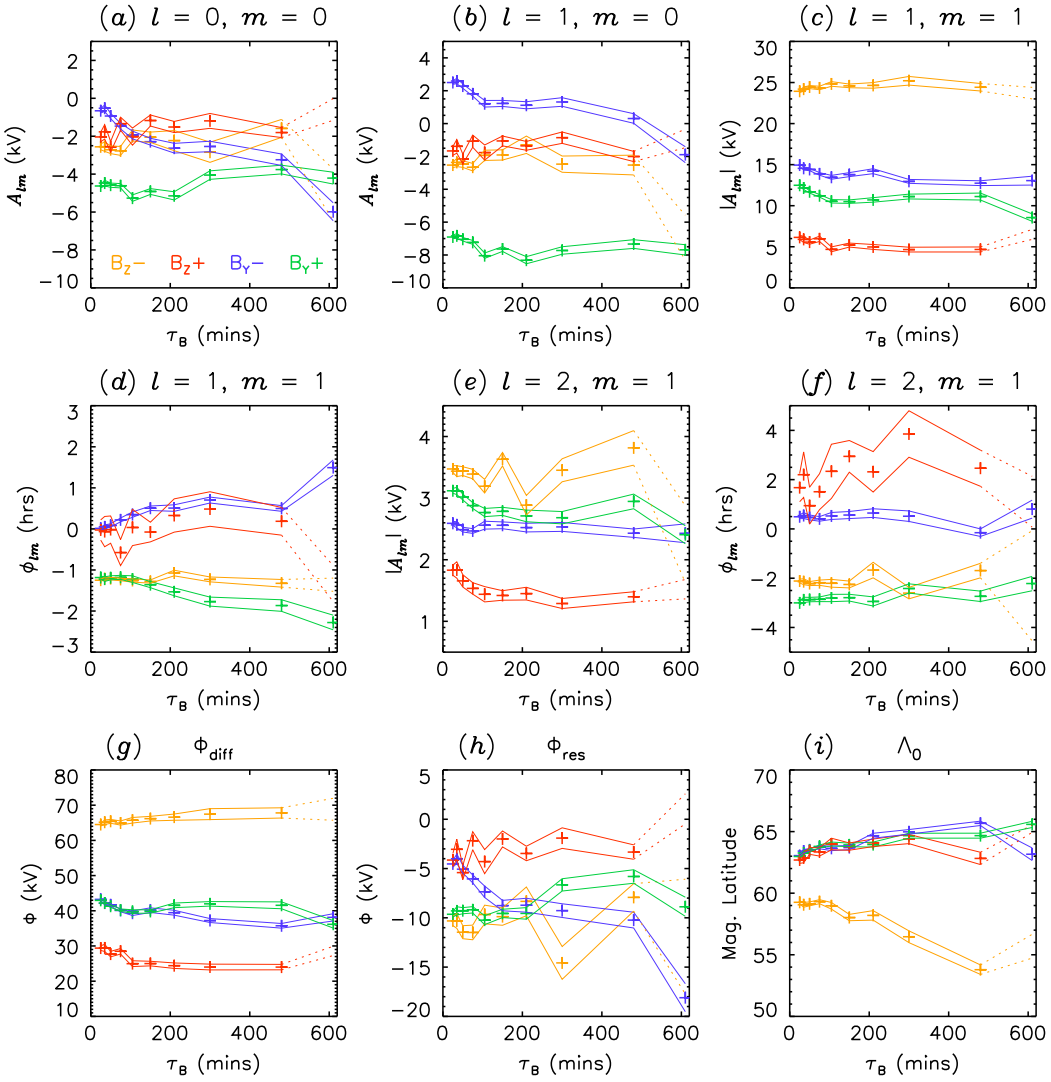

Figure 7. (a–f) Time series of coefficients of the spherical harmonic expansion of the ionospheric electric potential, plotted as a function of τ_B. The $A_{l,m}$ coefficients correspond to the zeroth-degree basis functions. The higher-degree coefficients have been resolved into a magnitude, $|A_{l,m}|$, and phase, $\phi_{l,m}$. In each case, the corresponding l and m values are shown at the top of each panel. (g) The maximum potential difference (between the maximum and minimum potentials) and (h) the residual potential (the sum of the maximum and minimum potentials). Shown in Figure 7f is the latitude of the equatorward boundary of the convection, Λ_0. Colored crosses represent mean values for each τ_B bin for the IMF sectors 1 (B_Z-: orange), 6 (B_Y-: blue), 9 (B_Z+: red), and 12 (B_Y+: green). The solid lines provide an estimate of the upper and lower 95% confidence intervals for the means.

Figure 7, we can draw some quantitative conclusions regarding the effects of τ_B on the convection pattern and hence on the associated magnetospheric dynamics.

Consider the $l = 0$ coefficients in Figure 7a. These show that for IMF-B_Y-, the magnitude of $A_{l,m}$ increases (to larger negative values) with increasing τ_B. This implies that in this case, the negative potential in the convection pattern becomes more enhanced as the IMF timescale increases. This is consistent with the corresponding increase in negative residual shown in Figure 7h. For IMF-B_Y+ on the other hand, there is little evidence of a convincing trend with increasing τ_B. Instead, the negative bias, which is already present at smaller τ_B, remains largely constant. A weak trend for the potential to become less negative may exist, but this is certainly less significant than the B_Y- case. For the B_Z-dominated IMF cases (sectors 1 and 9), the negative potential bias is small for all regimes of τ_B. This implies that the negative bias is very much an IMF-B_Y related phenomenon. A similar pattern exists for the $A_{1,0}$ coefficients in Figure 7b, although the weak B_Y+ trend is, if anything, reversed in this case.

Next we focus on the morphology of the "twin vortex" basis function, described by $A_{1,1}$, shown in Figures 7c and 7d. For B_Z-, there is little evidence for a dependence of $A_{1,1}$ on τ_B. Interesting to note, however, is that Φ_{diff} (Figure 7e) does show a modest increase with increasing τ_B. This implies that other basis functions better represent the increased flows contributing to the increase in Φ_{diff} in this case. For B_Z+, $|A_{1,1}|$ remains small for all IMF timescales, whereas $\phi_{1,1}$ shows considerable variability across the different τ_B bins. For both B_Y-dominated cases, $|A_{1,1}|$ decreases with increasing τ_B. The most significant evolution in these cases, however, is in $\phi_{1,1}$. For $20 < \tau_B < 30$ min, the rotation offset between the two B_Y orientations is 1 h. Moving to larger τ_B, this offset grows to ~4 h, with a clear positive (anticlockwise) rotation of the basis function developing for B_Y- and a negative (clockwise) rotation for B_Y+.

Finally, we illustrate the behavior of the higher-order basis functions, by considering the $A_{2,1}$ coefficients, shown in Figures 7e and 7f. Little trend is evident in the IMF-B_Y dominant and B_Z- cases, but there is some evidence for an evolution of the coefficients under B_Z+. The magnitude of the coefficient is shown to decrease for τ_B up to 6 h. At the same time, the phase ($\phi_{2,1}$) indicates an increasing rotation of the corresponding basis function which, according to *Grocott et al.* [2012], is the signature of the reverse convection cells. It is worth noting, however, the significant uncertainty on this set of coefficient means in particular. This suggests that even when ordering the convection by IMF clock angle, magnitude, and timescale, it still exhibits considerable variability. This is considered further in section 3.3. The other higher-order coefficients (not shown) exhibit even more variability, likely resulting from additional fine-scale structure in the individual convection intervals, which we leave consideration of to future studies.

3. Discussion

The observations described above show that, in addition to the expected dependencies on IMF orientation reported by numerous authors [e.g., *Heppner and Maynard*, 1987; *Rich and Hairston*, 1994; *Weimer*, 1995; *Ruohoniemi and Greenwald*, 1996, 2005], the nature of the high-latitude ionospheric convection pattern is also dependent on the length of time over which a given IMF orientation has been dominant at the magnetopause. We have defined a parameter, τ_B, to quantify this "steadiness timescale," and its significance can be readily explained by the idea that, rather than simply changing from one mode of dynamics to another, the magnetosphere integrates the effects of solar wind-magnetosphere coupling, evolving as the effects of that coupling become intensified over time. For such effects to become apparent, τ_B must be greater than the 10–15 min taken for changes in dayside solar wind-magnetosphere coupling to propagate over the polar cap [e.g., *Lockwood et al.*, 1986; *Etemadi et al.*, 1988; *Todd et al.*, 1988; *Saunders et al.*, 1992; *Khan and Cowley*, 1999], and greater than the few hour timescales over which ionospheric dynamics directly associated with tail processes, such as magnetospheric substorms, dominate [e.g., *Lester et al.*, 1993; *Hairston and Heelis*, 1995; *Grocott et al.*, 2002, 2010]. As mentioned in section 1, previous studies have accounted for the former by using 10–40 min intervals of the IMF either averaged, or inspected, to ensure a quasi-steady state has been approached [e.g., *Heppner and Maynard*, 1987, *Weimer*, 1995; *Ruohoniemi and Greenwald*, 1996; *Shepherd et al.*, 2002; *Ruohoniemi and Greenwald*, 2005]. Such studies average out any longer timescale effects, and it is these effects we consider here, for the different IMF orientations, B_Z-, B_Z+, and B_Z+ with $|B_Y| > B_Z$.

3.1. Southward IMF

There were two primary findings of our study into the convection pattern evolution under southward IMF conditions. The first was that the general shape of the convection pattern showed little evidence of any evolution. Even IMF sectors 4 and 14 (shown in the supporting information), which represent the most B_Y dominant of the southward IMF sectors, show no discernible dependence on τ_B. Given that we expect substorms to dominate the magnetospheric response to solar wind driving under these conditions [*Grocott et al.*, 2009], we might also expect some substorm-related asymmetry to be introduced [e.g., *Grocott et al.*, 2010]. However, the timescales for substorm recurrence are variable [e.g., *Freeman and Farrugia*, 1999], so any asymmetry may be averaged out by our analysis method. Average convection patterns derived with respect to substorm epoch, such as those produced by *Grocott et al.* [2010], rather than being defined relative to τ_B, might therefore be more appropriate in this case.

The second finding was that the latitudinal extent of the convection pattern increased with increasing τ_B. If a change in the size of the convection pattern is taken as a proxy for a change in the size of the open polar cap [e.g., *Imber et al.*, 2013], this implies that, on average, a modest southward IMF will cause a net

increase in the amount of open magnetic flux over timescales of many hours. Over such long timescales, this is unlikely to be attributable to the simple oscillation in open flux content that is expected from the substorm cycle, which might occur on timescales of tens of minutes to a few hours. Instead, it appears that long-term exposure to southward IMF will result in an overall imbalance between dayside and nightside reconnection. In other words, without fluctuations in the dayside coupling that might interrupt the addition of open flux to the magnetotail, nightside reconnection processes do not react sufficiently to close all of the flux being opened at the dayside. This idea is consistent with established ideas on the morphology of the polar cap during prolonged intervals of southward IMF such as those that occur during geomagnetic storms. *Milan et al.* [2009] demonstrated that the intensification of the ring current during the main phase of a geomagnetic storm plays an important role in determining the threshold of open flux (and hence polar cap size) at which substorms act to reduce this size. *Hutchinson et al.* [2011a] showed that for coronal mass ejection-driven storms, the main phase of a storm can take ~500 min to develop, and for corotating interaction region-driven storms, it may take well over 1000 min. Clearly, such timescales must be taken into account in order to fully characterize the morphology of the associated convection pattern.

It was noted above that the behavior of $|A_{1,1}|$ (Figure 7c), which provides a measure of the strength of the twin vortex component of the convection pattern, shows little dependence on τ_B. This suggests that the strength of the twin vortex is not dependent on the timescale over which it is driven. In fact, there is some evidence for a modest increase in $|A_{1,1}|$ for the first few τ_B bins, up to timescales of ~60 min. This is consistent with the timescales discussed above, over which both dayside and nightside reconnection will become established to drive the overall convection pattern. Beyond this, while the net amount of open flux in the polar cap may continue to grow (and result in an expansion of the convection pattern), owing to an imbalance between dayside and nightside reconnection rates, it is the overall rate of flux throughput that governs the strength of the convection [e.g., *Lockwood*, 1991]. This rate is understood to be directly related to the instantaneous upstream interplanetary conditions [*Shepherd et al.*, 2002] and would therefore not be expected to evolve over longer timescales if the upstream conditions remained the same.

Although dusk-dawn asymmetries in the convection pattern are generally attributed to IMF B_Y [e.g., *Ruohoniemi and Greenwald*, 1995], it is apparent, from this and numerous other studies [e.g., *de la Beaujardière et al.*, 1991; *Weimer*, 1995; *Ruohoniemi and Greenwald*, 1996], that there exists a dawn-dusk asymmetry in the convection pattern even for the strictly southward IMF case. Both a rotation of the convection pattern by ~1 h, and a bias toward a stronger negative potential cell by ~10 kV, exist. There is no evidence for the rotation of the pattern to lessen over any timescale (see, e.g., Figure 7d), suggesting that it is not just an artifact of some prior IMF B_Y influence. It may instead be an intrinsic asymmetry in the system resulting from the latitudinal gradient of the height-integrated Hall conductivity associated with the auroral oval conductivity enhancement [*Barbosa*, 1985] or the conductivity gradient between the dayside and nightside ionosphere [*Atkinson and Hutchison*, 1978]. There is some evidence that the negative potential bias gradually reduces if the IMF remains in a $B_Y \sim 0$ orientation for some time (e.g., Figures 7a–7b); however, this effect is small and may not be significant.

3.2. Northward IMF With a Dominant B_Y Component

The results presented in section 2.2.2 suggest that the IMF timescale has a much stronger effect on the shape of the convection pattern when the IMF is northward than when it is southward. Comparison of the $B_Z + /B_Y-$ and $B_Z + /B_Y+$ patterns in Figure 3 (top left and top right panels, respectively) with the $\tau_B > 600$ min panels of Figures 5a and 5b, reveals that the averaging employed by, e.g., *Ruohoniemi and Greenwald* [2005] masks certain characteristics of the convection that arise only after many hours of solar wind driving with a steady IMF orientation. In particular, the effects of increased τ_B in these cases can be summarized as an increased rotation of the twin vortex away from the noon-midnight meridian and a change in the distribution of the potential between the positive and negative potential cells. This is also evident in the basis function coefficients shown in Figure 7 and described in section 2.3. In addition, with the exception of the largest τ_B in the B_Z+/B_Y- case (Figure 5b (bottom right)), the size of the convection pattern appears to decrease with increasing τ_B (see also Figure 7i).

The enhanced rotational dusk-dawn asymmetries observed for large τ_B have been observed previously in studies of tail reconnection during IMF northward, nonsubstorm intervals (TRINNIs) [*Grocott et al.*, 2007]. Although bursty in nature, this phenomenon tends to occur over extended intervals of intermediate IMF clock angle ($\theta \sim 30°$). *Grocott et al.* [2007] showed that the asymmetric convection pattern is consistent

with a twist having developed in the tail as a result of persistent dayside open flux production via reconnection with the B_Y-dominated IMF [e.g., *Cowley*, 1981]. Recent MHD modeling studies into the effects of tail twisting have suggested that many hours are required for such effects to fully evolve [e.g., *Wang et al.*, 2014]. In our theoretical model, closed tail field lines, having foot points displaced in azimuth as a result of the tail twist, convect earthward and duskward/dawnward as they form the return flow of the convection cycle, giving rise to the azimuthal flows across the midnight sector ionosphere. These effects conspire to produce convection patterns that strongly resemble those depicted in each of Figures 5a (bottom right) and 5b (bottom right). Unlike the seasonal dependence of the asymmetry which, in winter, is expected to rotate the patterns toward later local times irrespective of the sign of IMF B_Y [e.g., *de la Beaujardière et al.*, 1991; *Pettigrew et al.*, 2010], we find an increased rotation toward later/earlier local times that is dependent of the sign of B_Y. This effect is demonstrated by the blue and green lines in Figure 7d. This is the first time that a characteristic timescale for the development of a dominant TRINNI convection pattern has been quantitatively investigated.

A statistical study of these azimuthal, nightside, ionospheric flows by *Grocott et al.* [2008] revealed them to be associated with only low levels of geomagnetic activity, implying that they are a distinct phenomenon, unrelated to substorms. Given the low level of solar wind driving expected in association with the northward IMF, *Grocott et al.* [2003] hypothesized that rather than being driven into the substorm cycle, the magnetosphere was responding in this case to a modest open flux production via periodic bursts of tail reconnection at a distant tail neutral line. This would facilitate the introduction of a twist into the tail and explain the quasi-constant size of open polar cap which would, in the absence of ongoing dayside open flux creation, be expected to shrink significantly over the 10 h timescale considered here [e.g., *Cowley and Lockwood*, 1992]. In fact, as noted above, there is evidence for a slight reduction in the size of the polar cap with increasing τ_B; the equatorward extent of the convection pattern decreases, in general, in both the B_Y+ and B_Y- cases. This might imply that on average, the nightside reconnection rate does exceed the dayside rate under these conditions. Exactly why this does not appear to hold true for the largest τ_B bin in the B_Y- case is unclear, but could be related to radar data coverage in this bin; Figure 1b shows that there is a bigger difference in coverage between the two largest τ_B bins in the B_Y- case than in the B_Y+ case.

An additional feature of the convection patterns that is apparent from this analysis is the difference in size and magnitude between the positive and negative potential cells. This is particularly noticeable when IMF B_Y is negative, where the dawn cell almost completely disappears for large τ_B; although there is some evidence for a similar change when B_Y is positive, it is much less apparent in this case. It is worth noting that there is a potential mismatch even for small τ_B; the positive (dawn) cell tends to be weaker all the time. *Watanabe et al.* [2007] suggested that the potential mismatch could arise from overdraped lobe field lines reconnecting with either dawnside or duskside closed flankside field lines. This could introduce a dusk-dawn asymmetry, although it is unclear why the duskside should be favored over the dawnside in all cases. Another possibility is that the day-night conductivity gradients discussed above also produce a dusk-dawn potential mismatch [e.g., *Lyatsky et al.*, 1974; *Ridley et al.*, 2004], causing the dusk cell potential to be larger than that of the dawn cell. Indeed, *Crooker and Rich* [1993] confirmed that this should be a winter phenomenon, such that the slight increase in winter bias for our large τ_B bin, discussed in section 2.1, could be an additional factor contributing to the larger, dominant dusk cell potential for B_Y-. However, *Papitashvili and Rich* [2002] and *Pettigrew et al.* [2010] suggest that in Northern Hemisphere winter, under B_Y+ conditions, the dawn cell should strengthen with respect to summer. This is not reflected in our results for B_Y+ and large τ_B, which is then inconsistent with a seasonal effect in this case. Overall our results, and those of previous studies, serve to demonstrate the complicated nature of the different dependencies of ionospheric convection asymmetries on a variety of factors that clearly warrant further, more in depth investigation.

3.3. Strictly Northward IMF

It has long been expected that during intervals of strongly northward IMF, twin reverse convection cells should appear in the high-latitude ionosphere in association with lobe reconnection [e.g., *Dungey*, 1963; *Crooker*, 1992]. There have been a number of reported observations of such flows [e.g., *Burke et al.*, 1979; *Heelis et al.*, 1986; *Cumnock et al.*, 1995; *Imber et al.*, 2006], but attempts to derive climatological patterns that well represent their morphology have had mixed success [e.g., *Ruohoniemi and Greenwald*, 1996; *Weimer*, 1995; *Ruohoniemi and Greenwald*, 2005; *Förster et al.*, 2008]. In Figure 6, we showed that, while there is definite evidence for the establishment of twin reverse cells even for small τ_B, they appear most strongly in the convection pattern derived for the 4–6 h τ_B bin. This suggests that the continued exposure to a strongly

northward IMF may be related to the morphology of these cells. It should be noted that the analysis of the spherical harmonic coefficients (presented in Figure 7) revealed little evidence for any convincing trends in the lower-order basis functions. This is perhaps to be expected, given that multicell patterns are known to be controlled by the higher-order functions [*Grocott et al.*, 2012]. This was hinted at by the response of the $|A_{2,1}|$ coefficients, which showed a significant dependence on τ_B up to 6 h.

To address why this might be so, we first consider again the possibility of a seasonal effect in controlling the appearance of the high-latitude cells. The reduced statistics for our long timescale bins introduces the possibility that the seasonal bias (toward winter) might become more significant in these cases. According to *Pettigrew et al.* [2010], however, the high-latitude reverse cells ought to be less pronounced in winter, not more pronounced as we find, suggesting that the dipole tilt is not responsible for the effect we observe.

Next we consider the possibility of ongoing nightside reconnection influencing the morphology of the convection. We presume that there is some ongoing nightside reconnection for two reasons. The first is that we expect nightside reconnection to continue, following a northward turning of the IMF; dayside open flux creation might turn off but we expect the tail will continue to close at least a portion of the pre-existing open flux [e.g., *Cowley and Lockwood*, 1992]. Furthermore, ongoing tail reconnection could explain the observed delay in the appearance of the strongest reverse cells. Certainly, we expect the reverse flows to appear on timescales of a few minutes following a northward turning off the IMF [e.g., *Ruohoniemi et al.*, 1993; *Imber et al.*, 2007]. However, ongoing nightside reconnection should produce a traditional twin vortex [*Cowley and Lockwood*, 1992; *Grocott et al.*, 2002] which would likely overwhelm comparatively weak reverse flows in the polar cap, suppressing them to some extent. Then, as the tail reconnection subsides following a prolonged drought of new open flux, the traditional twin vortex would weaken to leave the reverse twin vortex behind. Indeed, this is evidenced by the reduced size and potential of the lower-latitude twin vortex in the 4–6 h τ_B bin convection pattern.

One potential concern with this theory is whether the timescales involved are consistent with ongoing tail reconnection. It takes about 6 h for the high-latitude reverse convection cells to reach their strongest. The very small difference in the size of the convection pattern (indicated by a latitude change of about 1°) between the shortest and longest timescales raises the question of whether 6 h of persistent tail reconnection would leave such an expanded polar cap. A simple calculation suggests that the ~1° contraction observed corresponds to a net flux closure of only about 0.05 GWb. If this occurred over 6 h, and if we assume a linear decrease in the nightside reconnection rate over this time, then we find an initial rate of between just 2 kV and 5 kV. Any lower, and the rate would have to increase in order to close 0.05 GWb of flux in 6 h. Any higher, and it would have to decrease nonlinearly to still be decreasing after 6 h. It seems unlikely that the appearance of the reverse cells would be sensitive to such a small change in reconnection rate.

A number of other possible factors may be contributing to the delayed appearance of the strongest reversed convection cells. One could be related to the ionospheric wind dynamo, which could be maintaining the B_Z-negative twin vortex for a few hours after low-latitude dayside and nightside reconnection switches off [e.g., *Richmond and Matsushita*, 1975; *Richmond*, 1989]. During this time, the magnetospheric counterpart to these flows would become inductively decoupled as the magnetosheath end of the magnetic field lines are stretched further downstream by the solar wind [e.g., *Lockwood et al.*, 1990]. This decoupling of the ionosphere and magnetosphere could also be related to the fact that spacecraft have tended to observe the magnetospheric counterpart to reverse cell convection with more success than ground-based ionospheric observations. *Förster et al.* [2008], for example, presented clear evidence for twin reverse cells appearing in Cluster Electron Drift Instrument data after only 20 min of steady northward IMF. Lastly, it is evident from the larger uncertainty in the coefficient means presented in, for example, Figure 7f that the nature of the convection for strongly positive IMF-B_Z is highly variable. This was shown to be true when ordering the convection by IMF clock angle and magnitude [*Grocott et al.*, 2012], and it would seem to hold true when ordering by IMF timescale as well. It is likely, therefore, that the apparent weakness of the reverse convection cells in our average patterns is due not only to a superposition of geophysical effects competing at the same time but to our averages containing data from a superposition of time intervals, during which different geophysical effects were dominating despite the IMF conditions being similar in each case. A complete description of the convection for strongly northward IMF therefore requires further work that is outside the scope of the present study.

4. Summary

We have investigated the timescales of interplanetary magnetic field (IMF) control of ionospheric convection. We find that the nature of the ionospheric convection changes with IMF clock angle, as expected from previous time-averaged studies, and that for short intervals of steady IMF, the convection patterns closely resemble these time-averaged results. However, we also find that the patterns evolve, with increasing "IMF steadiness timescale," to less resemble their time-averaged counterparts. In particular, we find the following:

1. For southward IMF, the only discernible change with increasing steadiness timescale is an increase in the size of the convection pattern.
2. For northward/dawnward IMF, the orientation of the pattern rotates anticlockwise with increasing steadiness timescale such that the antisunward flow also has a dawnward component. The mismatch between the dusk and dawn (positive and negative) potential cells also increases such that the dusk cell becomes more dominant.
3. For northward/duskward IMF, the orientation of the pattern rotates clockwise with increasing steadiness timescale such that the antisunward flow becomes more strongly aligned toward dusk. In this case, the change in the dusk and dawn cell potentials is less clear, but overall the strength of both cells weakens.
4. For strongly northward IMF, the pattern shows a small reduction in size with increasing steadiness timescale. In addition, the reverse twin vortex flows expected under such IMF conditions become more pronounced, becoming strongest after 4–6 h.

We interpret these results as providing evidence for the interruption of direct solar wind control of the coupled magnetosphere-ionosphere system by strongly time-dependent internal magnetospheric and ionospheric processes. They serve to demonstrate the inherent inadequacy of ordering the high-latitude ionospheric convection by static parameters and the importance of the time history of the coupled solar wind-magnetosphere-ionosphere system in controlling the instantaneous dynamics.

Acknowledgments

The authors would like to acknowledge M.P. Freeman for helpful discussion. A.G. and S.E.M. were supported by NERC grant NE/G019665/1. SuperDARN data employed in this study are from radars that were funded at the time of operation by the research agencies of Japan, Canada, the U.S., France, and the UK and are available on request from the SuperDARN principal investigators. SuperDARN analysis software is available from the SuperDARN website (http://vt.superdarn.org). The ACE interplanetary magnetic field data used to bin the radar data are available from the NASA Space Physics Data Facility (http://cdaweb.gsfc.nasa.gov). Analysis code used to derive the results presented in this paper is available on request from the authors.

Michael Liemohn thanks Daniel Weimer and another reviewer for their assistance in evaluating this paper.

References

Atkinson, G., and D. Hutchison (1978), Effect of day night ionospheric conductivity gradient on polar-cap convective flow, *J. Geophys. Res*, *83*, 725–729.

Baker, D. N., T. I. Pulkkinen, V. Angelopoulos, W. Baumjohann, and R. L. McPherron (1996), Neutral line model of substorms: Past results and present view, *J. Geophys. Res.*, *101*, 12,975–13,010, doi:10.1029/95JA03753.

Barbosa, D. D. (1985), Polar convection patterns under quiet conditions, *J. Geophys. Res.*, *90*(A10), 9711–9716, doi:10.1029/JA090iA10p09711.

Burke, W. J., M. C. Kelley, R. C. Sagalyn, M. Smiddy, and S. T. Lai (1979), Polar cap electric-field structures with a northward interplanetary magnetic field, *Geophys. Res. Lett.*, *6*, 21–24.

Chisham, G., et al. (2007), A decade of the Super Dual Auroral Radar Network (SuperDARN): Scientific achievements, new techniques and future directions, *Surv. Geophys.*, *28*, 33–109, doi:10.1007/s10712-007-9017-8.

Cowley, S. W. H. (1981), Magnetospheric asymmetries associated with the Y-component of the IMF, *Planet. Space Sci.*, *29*(1), 79–96.

Cowley, S. W. H., and M. Lockwood (1992), Excitation and decay of solar wind-driven flows in the magnetosphere-ionosphere system, *Ann. Geophys.*, *10*, 103–115.

Cowley, S. W. H., et al. (2003), Solar-wind-magnetosphere-ionosphere interactions in the Earth's plasma environment, *Philos. Trans. R. Soc. London, Ser. A*, *361*, 113–126.

Crooker, N. U. (1992), Reverse convection, *J. Geophys. Res.*, *97*, 19,363–19,372.

Crooker, N. U., and F. J. Rich (1993), Lobe cell convection as a summer phenomenon, *J. Geophys. Res*, *98*(A8), 13,403–13,407, doi:10.1029/93JA01037.

Cumnock, J. A., R. A. Heelis, M. R. Hairston, and P. T. Newell (1995), High-latitude ionospheric convection pattern during steady northward interplanetary magnetic field, *J. Geophys. Res.*, *100*, 14,537–14,555.

de la Beaujardière, O., D. Alcayde, J. Fontanari, and C. Leger (1991), Seasonal dependence of high-latitude electric fields, *J. Geophys. Res.*, *96*(A4), 5723–5735, doi:10.1029/90JA01987.

Dungey, J. W. (1961), Interplanetary magnetic field and the auroral zones, *Phys. Rev. Lett.*, *6*, 47–48, doi:10.1103/PhysRevLett.6.47.

Dungey, J. W. (1963), The structure of the ionosphere, or adventures in velocity space, in *Geophysics: The Earth's Environment,* pp. 505–550, edited by J. H. C. DeWitt and A. Lebeau, Gordon and Breach, New York.

Etemadi, A., S. W. H. Cowley, M. Lockwood, B. J. I. Bromage, D. M. Willis, and H. Luhr (1988), The dependence of high-latitude dayside ionospheric flows on the North-South component of the IMF—A high time resolution correlation-analysis using EISCAT POLAR and AMPTE UKS and IRM data, *Planet. Space Sci.*, *36*(5), 471–498.

Förster, M., S. E. Haaland, G. Paschmann, J. M. Quinn, R. B. Torbert, H. Vaith, and C. A. Kletzing (2008), High-latitude plasma convection during northward IMF as derived from in-situ magnetospheric Cluster EDI measurements, *Ann. Geophys.*, *26*(9), 2685–2700.

Freeman, M. P., and C. J. Farrugia (1999), Solar wind input between substorm onsets during and after the October 18–20, 1995, magnetic cloud, *J. Geophys. Res.*, *104*, 22,729–22,744.

Grocott, A., S. W. H. Cowley, J. B. Sigwarth, J. F. Watermann, and T. K. Yeoman (2002), Excitation of twin-vortex flow in the nightside high-latitude ionosphere during an isolated substorm, *Ann. Geophys.*, *20*, 1577–1601.

Grocott, A., S. W. H. Cowley, and J. B. Sigwarth (2003), Ionospheric flow during extended intervals of northward but B_Y-dominated IMF, *Ann. Geophys.*, *21*, 509–538.

Grocott, A., T. K. Yeoman, S. E. Milan, O. Amm, H. U. Frey, L. Juusola, R. Nakamura, C. J. Owen, H. Rème, and T. Takada (2007), Multi-scale observations of magnetotail flux transport during IMF-northward non-substorm intervals, *Ann. Geophys.*, *25*, 1709–1720.

Grocott, A., S. E. Milan, and T. K. Yeoman (2008), Interplanetary magnetic field control of fast azimuthal flows in the nightside high-latitude ionosphere, *Geophys. Res. Lett.*, *35*, L08102, doi:10.1029/2008GL033545.
Grocott, A., J. A. Wild, S. E. Milan, and T. K. Yeoman (2009), Superposed epoch analysis of the ionospheric convection evolution during substorms: Onset latitude dependence, *Ann. Geophys.*, *27*(2), 591–600.
Grocott, A., S. E. Milan, N. Sato, J. A. Wild, T. K. Yeoman, and A. S. Yukimatu (2010), Superposed epoch analysis of the ionospheric convection evolution during substorms: IMF B_Y dependence, *J. Geophys. Res.*, *115*, A00I06, doi:10.1029/2010JA015728.
Grocott, A., S. E. Milan, S. M. Imber, M. Lester, and T. K. Yeoman (2012), A quantitative deconstruction of the morphology of high-latitude ionospheric convection, *J. Geophys. Res.*, *117*, A05317, doi:10.1029/2012JA017580.
Hairston, M. R., and R. A. Heelis (1995), Response-time of the polar ionospheric convection pattern to changes in the north-south direction of the IMF, *Geophys. Res. Lett.*, *22*(5), 631–634, doi:10.1029/94GL03385.
Heelis, R. A., P. H. Reiff, J. D. Winningham, and W. B. Hanson (1986), Ionospheric convection signatures observed by DE-2 during northward interplanetary magnetic field, *J. Geophys. Res.*, *91*, 5817–5830.
Heppner, J. P., and N. C. Maynard (1987), Empirical high-latitude electric-field models, *J. Geophys. Res.*, *92*(A5), 4467–4489.
Hones, E. W. (1979), Transient phenomena in the magnetotail and their relation to substorms, *Space Sci. Rev.*, *23*(3), 393–410.
Hutchinson, J. A., D. M. Wright, and S. E. Milan (2011a), Geomagnetic storms over the last solar cycle: A superposed epoch analysis, *J. Geophys. Res.*, *116*, A09211, doi:10.1029/2011JA016463.
Hutchinson, J. A., D. M. Wright, S. E. Milan, A. Grocott, and P. D. Boakes (2011b), A new way to study geomagnetic storms, *Astron. Geophys.*, *52*(4), 4–20.
Imber, S. M., S. E. Milan, and B. Hubert (2006), The auroral and ionospheric flow signatures of dual lobe reconnection, *Ann. Geophys.*, *24*, 3115–3129.
Imber, S. M., S. E. Milan, and B. Hubert (2007), Observations of significant flux closure by dual lobe reconnection, *Ann. Geophys.*, *25*(7), 1617–1627.
Imber, S. M., S. E. Milan, and M. Lester (2013), The Heppner-Maynard boundary measured by SuperDARN as a proxy for the latitude of the auroral oval, *J. Geophys. Res. Space Physics*, *118*, 685–697, doi:10.1029/2012JA018222.
Khan, H., and S. W. H. Cowley (1999), Observations of the response time of high-latitude ionospheric convection to variations in the interplanetary magnetic field using EISCAT and IMP-8 data, *Ann. Geophys.*, *17*, 1306–1335, doi:10.1007/s005850050858.
Lester, M., O. de la Beaujardiere, J. C. Foster, M. P. Freeman, H. Lühr, J. M. Ruohoniemi, and W. Swider (1993), The response of the large-scale ionospheric convection pattern to changes in the IMF and substorms—Results from the Sundial 1987 campaign, *Ann. Geophys.*, *11*(7), 556–571.
Lockwood, M. (1991), On flow reversal boundaries and transpolar voltage in average models of high-latitude convection, *Planet. Space Sci.*, *39*(3), 397–409.
Lockwood, M., A. P. Vaneyken, B. J. I. Bromage, D. M. Willis, and S. W. H. Cowley (1986), Eastward propagation of a plasma convection enhancement following a southward turning of the interplanetary magnetic field, *Geophys. Res. Lett.*, *13*(1), 72–75, doi:10.1029/GL013i001p00072.
Lockwood, M., S. W. H. Cowley, and M. P. Freeman (1990), The excitation of plasma convection in the high-latitude ionosphere, *J. Geophys. Res*, *95*(A6), 7961–7972, doi:10.1029/JA095iA06p07961.
Lyatsky, W. B., Y. P. Maltsev, and S. V. Leontyev (1974), Three-dimensional current system in different phases of a substorm, *Planet. Space Sci.*, *22*(8), 1231–1247, doi:10.1016/0032-0633(74)90007-5.
Milan, S. E., J. A. Wild, A. Grocott, and N. C. Draper (2006), Space- and ground-based investigations of solar wind magnetosphere ionosphere coupling, *Adv. Space Res.*, *38*, 1671–1677, doi:10.1016/j.asr.2005.08.009.
Milan, S. E., G. Provan, and B. Hubert (2007), Magnetic flux transport in the Dungey cycle: A survey of dayside and nightside reconnection rates, *J. Geophys. Res.*, *112*, A01209, doi:10.1029/2006JA011642.
Milan, S. E., P. D. Boakes, and B. Hubert (2008), Response of the expanding/contracting polar cap to weak and strong solar wind driving: Implications for substorm onset, *J. Geophys. Res.*, *113*, A09215, doi:10.1029/2008JA013340.
Milan, S. E., J. Hutchinson, P. D. Boakes, and B. Hubert (2009), Influences on the radius of the auroral oval, *Ann. Geophys.*, *27*(7), 2913–2924.
Milan, S. E., A. Grocott, and B. Hubert (2010), A superposed epoch analysis of auroral evolution during substorms: Local time of onset region, *J. Geophys. Res.*, *115*, A00I04, doi:10.1029/2010JA015663.
Murr, D. L., and W. J. Hughes (2007), The coherence between the IMF and high-latitude ionospheric flows: The dayside magnetosphere-ionosphere low-pass filter, *J. Atmos. Terr. Phys.*, *69*, 223–233, doi:10.1016/j.jastp.2006.07.019.
Nishida, A. (1968), Coherence of geomagnetic DP-2 fluctuations with interplanetary magnetic variations, *J. Geophys. Res.*, *73*, 1795.
Papitashvili, V. O., and F. J. Rich (2002), High-latitude ionospheric convection models derived from defense meteorological satellite program ion drift observations and parameterized by the interplanetary magnetic field strength and direction, *J. Geophys. Res.*, *107*(A8), SIA 17-1–SIA 17-13, doi:10.1029/2001JA000264.
Parker, E. N. (1963), *Interplanetary Dynamical Processes*, Interscience Publishers, New York.
Pettigrew, E. D., S. G. Shepherd, and J. M. Ruohoniemi (2010), Climatological patterns of high‐latitude convection in the Northern and Southern Hemispheres: Dipole tilt dependencies and interhemispheric comparisons, *J. Geophys. Res.*, *115*, A07305, doi:10.1029/2009JA014956.
Rich, F. J., and M. Hairston (1994), Large-scale convection patterns observed by DMSP, *J. Geophys. Res.*, *99*(A3), 3827–3844, doi:10.1029/93JA03296.
Richmond, A. D. (1989), Modelling the ionosphere wind dynamo: A review, *Pure Appl. Geophys.*, *131*(3), 413–435.
Richmond, A. D., and S. Matsushita (1975), Thermospheric response to a magnetic substorm, *J. Geophys. Res*, *80*(19), 2839–2850, doi:10.1029/JA080i019p02839.
Ridley, A. J., G. Lu, C. R. Clauer, and V. O. Papitashvili (1998), A statistical study of the ionospheric convection response to changing interplanetary magnetic field conditions using the assimilative mapping of ionospheric electrodynamics technique, *J. Geophys. Res.*, *103*(A3), 4023–4039, doi:10.1029/97JA03328.
Ridley, A. J., T. I. Gombosi, and D. L. DeZeeuw (2004), Ionospheric control of the magnetosphere: Conductance, *Ann. Geophys.*, *22*(2), 567–584.
Ruohoniemi, J. M., and K. B. Baker (1998), Large-scale imaging of high-latitude convection with Super Dual Auroral Radar Network HF radar observations, *J. Geophys. Res.*, *103*, 20,797–20,811, doi:10.1029/98JA01288.
Ruohoniemi, J. M., and R. A. Greenwald (1995), Observations of IMF and seasonal effects in high-latitude convection, *Geophys. Res. Lett.*, *22*(9), 1121–1124.
Ruohoniemi, J. M., and R. A. Greenwald (1996), Statistical patterns of high-latitude convection obtained from Goose Bay HF radar observations, *J. Geophys. Res.*, *101*, 21,743–21,764, doi:10.1029/96JA01584.

Ruohoniemi, J. M., and R. A. Greenwald (1997), Rates of scattering occurrence in routine HF radar observations during solar cycle maximum, *Radio Sci.*, *32*(3), 1051–1070, doi:10.1029/97RS00116.

Ruohoniemi, J. M., and R. A. Greenwald (2005), Dependencies of high-latitude plasma convection: Consideration of interplanetary magnetic field, seasonal, and universal time factors in statistical patterns, *J. Geophys. Res.*, *110*, A09204, doi:10.1029/2004JA010815.

Ruohoniemi, J. M., R. A. Greenwald, O. de la Beaujardière, and M. Lester (1993), The response of the high-latitude dayside ionosphere to an abrupt northward transition in the IMF, *Ann. Geophysicae*, *11*(7), 544–555.

Saunders, M. A., M. P. Freeman, D. J. Southwood, S. W. H. Cowley, M. Lockwood, J. C. Samson, C. J. Farrugia, and T. J. Hughes (1992), Dayside ionospheric convection changes in response to long-period interplanetary magnetic field oscillations - Determination of the ionospheric phase-velocity, *J. Geophys. Res.*, *97*(A12), 19,373–19,380, doi:10.1029/92JA01383.

Sergeev, V. A., R. J. Pellinen, and T. I. Pulkkinen (1996), Steady magnetospheric convection: A review of recent results, *Space Sci. Rev.*, *75*(3–4), 551–604, doi:10.1007/BF00833344.

Shepherd, S., and J. Ruohoniemi (2000), Electrostatic potential patterns in the high-latitude ionosphere constrained by SuperDARN measurements, *J. Geophys. Res.*, *105*(A10), 23,005–23,014.

Shepherd, S. G., R. A. Greenwald, and J. M. Ruohoniemi (2002), Cross polar cap potentials measured with Super Dual Auroral Radar Network during quasi-steady solar wind and interplanetary magnetic field conditions, *J. Geophys. Res.*, *107*(A7), SMP 5-1–SMP 5-11, doi:10.1029/2001JA000152.

Smith, C. W., J. L'Heureux, N. F. Ness, M. H. Acuña, L. F. Burlaga, and J. Scheifele (1998), The ACE magnetic fields experiment, *Space Sci. Rev.*, *86*, 613–632, doi:10.1023/A:1005092216668.

Stone, E. C., A. M. Frandsen, R. A. Mewaldt, E. R. Christian, D. Margolies, J. F. Ormes, and F. Snow (1998), The advanced composition explorer, *Space Sci. Rev.*, *86*, 1–22, doi:10.1023/A:1005082526237.

Todd, H., S. W. H. Cowley, M. Lockwood, D. M. Wills, and H. Luhr (1988), Response-time of the high-latitude dayside ionosphere to sudden changes in the north-south component of the IMF, *Planet. Space Sci.*, *36*(12), 1415–1428.

Wang, J. Y., C. Wang, Z. H. Huang, and T. R. Sun (2014), Effects of the interplanetary magnetic field on the twisting of the magnetotail: Global MHD results, *J. Geophys. Res. Space Physics*, *119*, 1887–1897, doi:10.1002/2013JA019257.

Watanabe, M., G. J. Sofko, K. Kabin, R. Rankin, A. J. Ridley, C. R. Clauer, and T. I. Gombosi (2007), Origin of the interhemispheric potential mismatch of merging cells for interplanetary magnetic field B_y-dominated periods, *J. Geophys. Res.*, *112*, A10205, doi:10.1029/2006JA012179.

Weimer, D. R. (1995), Models of high-latitude electric potentials derived with a least error fit of spherical harmonic coefficients, *J. Geophys. Res.*, *100*(A10), 19,595–19,607, doi:10.1029/95JA01755.